1986ApJ...308..530F

THE ASTROPHYSICAL JOURNAL, 308:530–539, 1986 September 15
© 1986. The American Astronomical Society. All rights reserved. Printed in U.S.A.

AN X-RAY AND OPTICAL STUDY OF THE CLUSTER OF GALAXIES ABELL 754

D. FABRICANT, T. C. BEERS,[1] M. J. GELLER, P. GORENSTEIN, J. P. HUCHRA,[1] AND M. J. KURTZ[1]
Harvard-Smithsonian Center for Astrophysics[2]
Received 1985 December 23; accepted 1986 March 4

ABSTRACT

We use X-ray images from the *Einstein Observatory*, galaxy counts ($m_R \leq 17.8$) for the central region of the cluster, and galaxy redshifts to study the structure of A754, a dense, rich cluster of galaxies with an X-ray luminosity comparable to that of the Coma Cluster. The simplest mass distribution which can produce the smooth, flattened X-ray surface brightness profile is one in which the X-ray emitting gas is in hydrostatic equilibrium in the gravitational potential of two self-gravitating isothermal spheres. We use the V'/V'_{max} test to show that the galaxy counts are consistent with this mass distribution. The agreement of the optical and X-ray data indicates that on a scale of 0.5–1 Mpc ($H_0 = 100$ km s^{-1} Mpc^{-1}), the galaxies trace the averaged matter distribution in this system.

Subject headings: galaxies: clustering — X-rays: sources

I. INTRODUCTION

Both X-ray and optical data have provided increasingly detailed and convincing evidence for substructure in clusters of galaxies (e.g., Baier 1976; Forman *et al.* 1981; Geller and Beers 1982; Forman and Jones 1982). These departures from the canonical smooth system in virial equilibrium suggest that many clusters of galaxies retain the imprint of their initial conditions (Geller 1984; Cavaliere *et al.* 1985).

Many clumpy systems have a low central galaxy density and contain a high fraction of spiral galaxies (Abell 1958; Dressler 1980; Oemler 1974; Forman and Jones 1982; Bothun *et al.* 1983). In contrast, the cluster A754 is a dense system populated with S0 and elliptical galaxies (Dressler 1980). A754 and the Coma Cluster have similar galaxy densities and X-ray luminosities. Our analysis of the X-ray and optical data shows that A754 is, nonetheless, bimodal.

The dynamical history of clusters and the distribution of dark matter are closely tied together. We use the X-ray and optical data for A754 to study the relative distribution of the luminous and dark matter. In particular, we undertake a quantitative statistical comparison of the galaxy positions with the total mass responsible for maintaining the X-ray emitting gas in hydrostatic equilibrium. A simple bimodal model which fits both the X-ray and optical data suggests that the galaxies are distributed consistently with the projected matter distribution within the region covered by the X-ray map (0.5–1 Mpc).

II. THE X-RAY OBSERVATIONS

a) *Surface Brightness Map*

The X-ray data comprise two exposures from the *Einstein Observatory* data bank, an imaging proportional counter (IPC) exposure of 3114 s effective duration, and a high resolution imager (HRI) exposure of 5644 s effective duration. Because of the much higher quantum efficiency and much lower internal background of the IPC, we use the HRI exposure only for limiting the contributions from an F star in the field (for detailed properties of these intruments see Harnden *et al.* 1984; Harris 1984).

The standard procedure for constructing surface brightness maps of extended objects consists of binning the IPC data at the desired scale, subtracting an estimated background, correcting for the vignetting of the telescope optics, and applying the desired spatial smoothing. The routine *Einstein* data processing system accounts for spacecraft motion and applies corrections for nonlinearities in the spatial scale of the IPC and for gain variations over time and with position in the detection volume. Because of favorable orbital geometry, the A754 exposure requires no additional screening to eliminate the background variations caused by solar X-rays scattered by Earth's atmosphere.

The pulse height channels covering the 0.3–3.5 keV energy band give the optimum signal-to-noise ratio for typical cluster spectra with $kT > 3$ keV and with relatively low absorbing column densities along the line of sight. We bin the data in 0.′67 × 0.′67 pixels.

Similarly binned data from five high galactic latitude surveys in constant detector coordinates provide our estimate of the X-ray plus non–X-ray background. After normalizing by the ratio of observing times in the data and background exposures, and applying the appropriate average roll and offset motions to convert to celestial coordinates, the background array can be subtracted directly from the data array. By examination of the residuals at large distances from the cluster center, we estimate that the background level is correct to $\sim 20\%$.

The background-subtracted array is corrected for vignetting and is smoothed by convolution with a Gaussian with a 1.′6 FWHM; the resulting map has an effective resolution of 2.′2 when the intrinsic IPC spatial resolution of 1.′5 is added to the smoothing in quadrature. Figure 1 shows the surface brightness contours spaced by a constant factor of 1.5. The highest contour is 0.012 IPC counts cm^{-2} s^{-1} arcmin^{-2}, or 3.5×10^{-13} ergs s^{-1} cm^{-2} arcmin^{-2} in the 0.3–3.5 keV band. Corrected for absorption in our Galaxy, this level is equivalent to 4.2×10^{-13} ergs s^{-1} cm^{-2} arcmin^{-2}. These conversions from count rate to flux have been made assuming an 8 keV thermal spectrum and a Galactic hydrogen column density of 10^{21}. Heiles (1975) reports a value of $\sim 7 \times 10^{20}$ in this region. The lowest contour level is ~ 2.5 times the background level;

[1] Visiting Scientist, Kitt Peak National Observatory, which is operated by the Associated Universities for Research in Astronomy, Inc.

[2] Research reported here used the Multiple Mirror Telescope Observatory, a joint facility of the Smithsonian Institution and the University of Arizona.

© American Astronomical Society • Provided by the NASA Astrophysics Data System

1986ApJ...308..530F

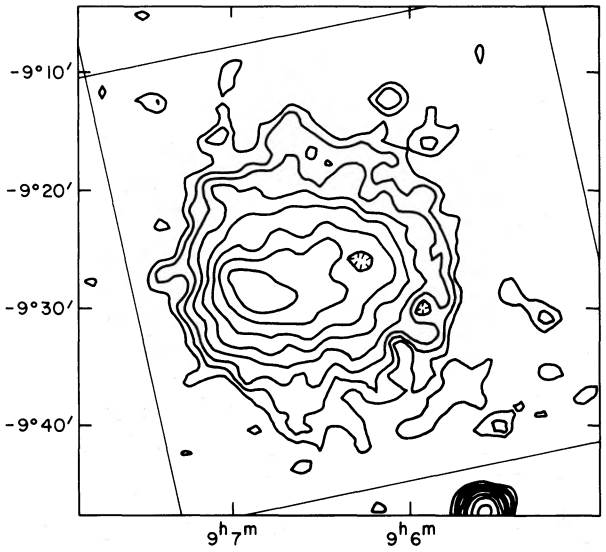

FIG. 1.—An 0.3–3.5 keV contour map of the X-ray surface brightness of A754. The surface brightness peaks at R.A. = $9^h6^m50^s$ and Decl. = −9°28′.5. Background has been subtracted and the map has been corrected for the vignetting of the telescope. The contour levels are separated by a factor of 1.5. The highest level plotted is 1.2×10^{-3} IPC counts s^{-1} arcmin^{-2} or 3.5×10^{-13} ergs cm^{-2} s^{-1} arcmin^{-2} in the 0.3–3.5 keV energy band (uncorrected for absorption in our Galaxy. The correction is a factor of ~1.2). For $H_0 = 100$ km s^{-1} Mpc^{-1}, the scale is 46.5 kpc arcmin^{-1}. The resolution of this map is 2′.2. The source southwest of A754 is associated with a radio galaxy located in a group of galaxies at approximately the same redshift as A754 (see Harris, Costain, and Dewdney 1984).

therefore, minor errors in background subtraction have a negligible effect on our results. After smoothing, the 1 σ fluctuations cause a ~30% variation in the level of the lowest contour and a 7% variation in the highest contour.

Figure 1 shows that the X-ray isophotes are pronouncedly elliptical. Furthermore, the peak of X-ray surface brightness is not concentric with the outer isophotes. We quantify the ellipticity and center of the eight plotted contours from the first and second moments of the plane figure bounded by each isophote. In order to minimize statistical fluctuations, we take the outer five isophotes from a version of the map smoothed to a lower resolution of ~3′.5 FWHM. In the outermost contour of this map, a 1 σ fluctuation is a 15% variation. Table 1 summarizes the axial ratios, the center of mass positions, and the position angles.

TABLE 1

RESULTS OF X-RAY ISOPHOTE ANALYSIS

Average Radius	Axial Ratio	Major Axis Position Angle (north to east)	Center Movement
2′.15.....	1.83	66°	0′.32
4.21.....	1.64	99	2.07
5.96.....	1.61	102	3.25
7.33.....	1.39	101	3.58
8.59.....	1.25	98	3.78
9.94	1.15	96	4.14
11.43.....	1.03	101	4.58
13.18.....	1.07	...	5.09

NOTE.—The tabulated results refer to isophotes separated by a factor of 1.5 in surface brightness; these are the same isophotes plotted in Fig. 1. The highest level corresponds to 0.0123 IPC counts s^{-1} arcmin^{-2}, or a flux of 4.2×10^{-13} ergs s^{-1} cm^{-2} arcmin^{-2} in the 0.3–3.5 keV energy band, corrected for absorption in our Galaxy.

X-ray emission from an 8.9 mag F star (HD 78665) located within 1′.5 of the peak X-ray surface brightness could, in principle, distort the moderate-resolution IPC map. However, the HRI exposure places sufficiently stringent limits to demonstrate that the contribution from the star is negligible. In an 18″ × 18″ region centered on the position of the F star, we detect 6 counts; the mean background including cluster emission (estimated from four regions of size 1′ × 1′ centered 1′ away from the star) is 5.5 ± 0.7 counts. At 90% confidence, the upper limit to the counts at the F star position is 11.8, yielding a conservative upper limit of 7 counts from the star. Multiplying by a factor of 0.56 for the relative observation lengths, and a factor of 2 for the relative efficiency of the IPC and HRI for soft spectra, we obtain an upper limit of 8 total IPC counts. At the 2′.2 resolution of the IPC map, the fractional contamination of the high surface brightness cluster center is less than 10%.

b) *Spectral Fits*

Low-resolution spatially resolved spectra are available from the IPC, but the relatively short exposure and high cluster temperature preclude useful results. The pulse height data from two regions of 3′ and 5′ radius surrounding the X-ray surface brightness peak are consistent with thermal spectra with $kT \gtrsim 1.5$ keV. For the integrated spectrum of the cluster, Mushotzky (1982) reports 90% confidence values of 8.2 ± 1.0 keV and 6.5 ± 1.0 keV from the *HEAO* A-2 xenon- and argon-filled proportional counters respectively. We adopt a temperature of 8 keV.

c) *Luminosity*

A754 is the sixth most luminous X-ray cluster in a sample of 74 Abell clusters (53 detections) studied by Abramopoulos and Ku (1983). For a thermal spectrum with $kT = 8$ keV, and a Galactic hydrogen column density of 10^{21}, the total (integrated over the entire 60′ × 60′ IPC field) luminosity is 2.2×10^{44} ergs s^{-1} in the 0.3–3.5 keV energy range ($H_0 = 100$ km s^{-1} Mpc^{-1}). For comparison, the luminosity of the Coma Cluster is within 25% of this value.

III. OPTICAL OBSERVATIONS

a) *The Photometric Data*

We obtained CCD calibrated photographic photometry in two colors (B and Kron-Cousins R) for the brighter galaxies within a 14′ × 30′ region surrounding the central condensation. We digitized a 4 × 4 cm region (45′ × 45′ on the sky) from the KPNO glass copies of Palomar Sky Survey plates E-728 and O-728 using the KPNO PDS machine with a 20 × 20 μm nonoverlapping aperture. We used the reduction procedure of Kurtz *et al.* (1985) with modifications described below.

Table 2 contains the positions and isophotal magnitudes for all galaxies in the region brighter than either $R = 17.8$ or $B = 19.0$. The limiting isophote is a function of the fluctuations in the background density on the plate. We calibrate the magnitudes by comparison with aperture magnitudes of galaxies in the center of the region obtained from two (one each in B and R) 1 hr CCD exposures with the 24 inch (61 cm) telescope on Mount Hopkins on 1982 April 19. The mean scatter about the calibrating relation is 0.14 mag in B and 0.17 mag in R (10

© American Astronomical Society • Provided by the NASA Astrophysics Data System

1986ApJ...308..530F

TABLE 2

GALAXY POSITIONS IN ABELL 754

R.A. (1950)	Decl.	R	B	Number[a]
$9^h5^m26^s5$	−9°28′33″	17.25	18.66	...
9 5 39.5	−9 24 36	17.42	19.04	...
9 5 43.6	−9 18 48	16.54	18.08	124
9 5 44.3	−9 19 41	16.45	17.89	110
9 5 44.3	−9 29 19	16.49	18.05	71
9 5 45.3	−9 25 12	16.82	18.30	...
9 5 47.2	−9 26 20	16.78	18.42	...
9 5 48.8	−9 18 07	15.67	17.15	122
9 5 49.1	−9 23 11	17.05	18.26	...
9 5 49.6	−9 24 49	15.92	17.44	93
9 5 50.6	−9 24 55	17.24	18.84	...
9 5 50.8	−9 26 20	16.73	18.35	...
9 5 50.8	−9 21 05	15.64	17.19	109
9 5 51.3	−9 31 25	15.44	17.08	60
9 5 51.6	−9 23 08	16.59	17.98	123
9 5 54.1	−9 22 54	16.71	18.22	...
9 5 55.3	−9 18 57	15.86	17.45	121
9 5 55.7	−9 27 05	16.85	18.62	...
9 5 56.1	−9 25 29	16.77	18.13	...
9 5 56.7	−9 25 55	16.30	17.83	95
9 5 57.1	−9 26 06	15.88	17.76	94
9 5 57.7	−9 22 30	17.57	19.03	...
9 5 58.0	−9 29 54	16.45	17.85	
9 5 58.4	−9 22 14	17.75	19.59	...
9 5 59.2	−9 21 21	16.54	18.47	...
9 5 59.5	−9 29 23	17.44	18.93	...
9 5 59.6	−9 26 00	17.58	19.16	...
9 5 59.7	−9 32 15	17.46	18.63	...
9 5 59.8	−9 22 45	17.04	18.37	...
9 5 59.9	−9 29 01	16.41	18.02	...
9 6 0.5	−9 27 00	16.63	18.14	...
9 6 0.5	−9 25 23	16.20	17.64	93
9 6 0.9	−9 21 26	15.78	17.18	108
9 6 1.4	−9 32 18	17.42	19.21	...
9 6 3.6	−9 24 46	16.23	17.88	...
9 6 5.1	−9 22 06	16.54	18.02	107
9 6 5.2	−9 26 10	14.94	16.63	92
9 6 5.4	−9 24 15	17.74	19.21	...
9 6 6.0	−9 24 54	17.09	18.81	...
9 6 6.2	−9 25 35	13.62	15.47	91
9 6 6.2	−9 18 23	16.51	18.02	...
9 6 7.0	−9 26 33	17.54	19.31	...
9 6 8.0	−9 32 06	17.64	20.05	...
9 6 8.0	−9 27 01	16.41	17.99	...
9 6 8.6	−9 28 31	17.40	18.97	...
9 6 9.1	−9 24 19	18.00	18.95	...
9 6 9.9	−9 25 06	16.11	17.73	...
9 6 11.4	−9 25 33	17.07	18.65	...
9 6 11.9	−9 24 14	16.93	18.61	...
9 6 12.3	−9 25 44	16.82	18.33	...
9 6 12.7	−9 25 16	15.61	17.22	90
9 6 12.9	−9 25 22	16.81	18.06	...
9 6 13.3	−9 28 10	17.00	18.51	...
9 6 15.1	−9 22 25	15.99	17.58	106
9 6 15.5	−9 21 06	17.55	18.93	...
9 6 16.2	−9 29 49	16.13	17.63	70
9 6 17.5	−9 23 56	15.99	17.56	89
9 6 17.6	−9 23 01	17.32	18.77	...
9 6 18.3	−9 21 48	17.15	18.66	...
9 6 21.9	−9 24 25	17.36	19.11	...
9 6 23.8	−9 25 35	17.45	18.63	...
9 6 24.1	−9 28 52	17.13	18.62	...
9 6 24.8	−9 23 22	15.79	17.37	105
9 6 26.8	−9 26 47	17.79	18.37	...
9 6 27.0	−9 27 25	16.96	18.29	...
9 6 27.2	−9 31 06	16.85	18.30	...
9 6 27.3	−9 27 18	17.62	19.09	...
9 6 27.5	−9 32 29	17.72	19.53	...
9 6 27.9	−9 26 43	16.29	17.81	...
9 6 28.0	−9 20 21	17.49	18.50	...
9 6 29.3	−9 28 33	15.04	16.64	69
$9^h6^m30^s1$	−9°23′41″	15.32	16.90	88
9 6 32.2	−9 23 46	14.96	16.44	87
9 6 32.4	−9 25 01	15.96	17.49	86
9 6 32.8	−9 25 39	16.47	18.07	...
9 6 33.7	−9 28 04	16.07	17.74	...
9 6 34.2	−9 23 16	16.76	18.25	...
9 6 34.3	−9 29 00	17.50	19.70	...
9 6 35.8	−9 25 26	16.54	18.13	...
9 6 36.5	−9 26 32	15.57	17.17	85
9 6 36.8	−9 21 57	17.70	18.55	...
9 6 37.8	−9 32 15	17.64	18.98	...
9 6 38.3	−9 31 58	16.10	17.70	59
9 6 38.7	−9 22 21	17.82	18.85	...
9 6 42.5	−9 23 19	17.67	18.86	...
9 6 42.9	−9 29 07	17.94	18.76	...
9 6 44.5	−9 29 59	17.24	19.25	...
9 6 44.5	−9 23 18	17.80	19.42	...
9 6 45.1	−9 30 29	17.10	18.58	...
9 6 45.5	−9 29 35	15.74	17.65	68
9 6 45.7	−9 27 06	17.61	19.08	...
9 6 46.0	−9 29 17	16.86	18.43	...
9 6 46.3	−9 34 03	15.72	17.13	58
9 6 46.8	−9 32 24	16.56	18.25	...
9 6 47.3	−9 26 01	16.29	17.81	84
9 6 48.3	−9 29 54	17.47	18.59	...
9 6 48.4	−9 35 53	16.66	18.43	...
9 6 49.1	−9 36 11	16.91	18.50	...
9 6 49.9	−9 32 07	17.33	19.29	...
9 6 50.1	−9 32 58	16.94	18.76	...
9 6 51.0	−9 32 16	16.32	18.09	...
9 6 51.6	−9 29 54	16.63	18.25	...
9 6 51.8	−9 36 53	16.72	18.27	...
9 6 51.9	−9 31 38	17.03	18.84	...
9 6 52.1	−9 34 10	17.63	18.98	...
9 6 52.1	−9 34 46	18.33	18.67	...
9 6 53.1	−9 29 46	14.68	16.33	67
9 6 54.0	−9 32 00	16.51	18.21	...
9 6 54.7	−9 31 22	16.02	17.61	57
9 6 54.9	−9 34 32	16.17	17.49	42
9 6 56.4	−9 35 03	17.23	18.69	...
9 6 56.5	−9 29 46	17.41	19.06	...
9 6 56.8	−9 31 45	16.41	18.02	...
9 6 57.6	−9 36 08	17.43	18.90	...
9 6 59.0	−9 33 03	17.62	18.48	...
9 6 59.1	−9 29 53	15.88	17.54	66
9 7 00.0	−9 35 05	17.30	18.34	...
9 7 0.4	−9 27 05	16.77	17.48	83
9 7 1.1	−9 25 41	15.29	16.86	82
9 7 1.9	−9 31 10	16.55	18.01	...
9 7 2.1	−9 29 00	15.72	17.35	65
9 7 2.9	−9 25 02	16.10	17.71	81
9 7 3.7	−9 30 15	17.10	18.74	...
9 7 4.7	−9 33 19	17.60	18.93	...
9 7 5.8	−9 35 01	16.82	18.29	...
9 7 7.6	−9 25 20	17.72	19.27	...
9 7 8.2	−9 28 53	16.90	18.38	...
9 7 8.3	−9 29 16	16.32	17.91	...
9 7 8.7	−9 32 55	15.52	17.17	55
9 7 8.8	−9 29 50	15.71	17.28	64
9 7 9.1	−9 33 50	15.48	17.03	56
9 7 9.7	−9 32 13	16.05	17.61	54
9 7 10.6	−9 26 06	16.40	18.06	...
9 7 11.6	−9 25 45	17.23	18.25	...
9 7 13.0	−9 31 10	14.76	16.32	53
9 7 16.8	−9 27 17	17.45	18.95	...
9 7 17.9	−9 30 18	15.98	17.58	63
9 7 17.9	−9 31 43	15.13	16.75	52
9 7 18.6	−9 26 21	16.41	18.03	80
9 7 19.6	−9 34 41	16.25	17.76	...
9 7 25.6	−9 31 52	17.35	18.77	...
9 7 32.7	−9 26 09	15.19	16.88	79

[a] Dressler 1980.

© American Astronomical Society • Provided by the NASA Astrophysics Data System

1986ApJ...308..530F

objects). The isophotal magnitudes should be very similar to large-aperture measurements (Kurtz *et al.* 1985). Because of the high degree of crowding (both because of the richness of the cluster and the low Galactic latitude), aperture measurements were not feasible, and most objects required some human judgment to estimate the total isophotal light. The field lies in the corner of the plate, where vignetting effects are greatest. However, the errors induced by differential vignetting in the sample region are expected to be considerably smaller than those in the photometry.

Scans in two colors permitted two independent star/galaxy classifications. All discrepant objects and objects with extreme colors were examined in detail. Because of these additional checks and the relatively bright limiting magnitude, the 143 galaxies in Table 2 should be more than 90% pure and complete, despite the unfavorable position of the cluster on the plate.

Figure 2 (Plate 11) shows isopleths from the data in Table 2 superposed on a reproduction of the PSS E plate showing the galaxies only. A reproduction of the PSS E plate of the entire $45' \times 45'$ region with the stars removed appears in Kurtz (1983).

According to the criterion of Geller and Beers (1982), the two maxima in Figure 2 are significant at the 3 σ level. A strip count along the major axis of the cluster also indicates bimodal structure significant at the 3 σ level. The cD or D galaxy at the peak of each of the concentrations (Dressler 1980) is additional evidence for substructure. Beers and Geller (1983) have shown that D galaxies mark the bottom of local potential wells.

Schecter (1976) functions with $m_R^* = 15.15$, $m_B^* = 16.75$, and $\alpha = -1.25$ fit the luminosity distribution for A754. The value of α is not well determined; the value of m^* changes by ± 0.20 as α changes by ± 0.25. Removal of the cD galaxy improves the fit, but the value of m^* is unchanged. With a distance modulus of 36.02, extinction corrections $A_B = 0.13$ and $A_R = 0.07$ (Burstein and Heiles 1982), and K-corrections of $K_B = 0.27$ and $K_R = 0.05$ (Schild and Oke 1971), we find M^* of $-19.67(B)$ and $-20.74(R)$, in good agreement with the values obtained from the CfA redshift survey (Davis and Huchra 1982).

The luminosity functions of the eastern and western (with the cD) clumps differ at the bright end. Figure 3 shows the comparison; the western clump is marginally deficient in bright galaxies, but not in faint ones. This would be expected if cD galaxies preferentially cannibalized their brighter neighbors. However, 1 hr R and B CCD frames taken with the 24 inch telescope on 1982 April 22 and 23 show no trace of multiple nuclei in the cD.

The colors of the galaxies are normal; the median color is $B-R = 1.56$, typical for S0 and elliptical galaxies with the indicated reddening and K-corrections. The color distributions in the western and eastern clumps are identical.

The total background subtracted light (Beers, Huchra, and Geller 1982) from measured galaxies in the region is $\sim 5 \times 10^{11}\ L_\odot$ in B and $\sim 7 \times 10^{11}\ L_\odot$ in R. With a velocity dispersion of 750 km s^{-1} (see § III*b*), we obtain a virial mass for the region $3.6 \pm 0.5 \times 10^{14}\ M_\odot$, in good agreement with the results of the X-ray analysis in § IV. Correcting the measured blue light by a factor of 1.3 to account for the light in faint galaxies (Davis and Huchra 1982), we obtain a mass-to-light ratio for the blue light, in solar units, of $M/L_B = 550$.

b) The Spectroscopic Data

We have measured redshifts for 17 galaxies in the region of A754. Medium-resolution spectra were obtained with the photon-counting Reticon system at the Multiple Mirror Telescope (Latham 1979). A 300 lines mm^{-1} grating was used in first order, giving a resolution of ~ 8 Å, over a wavelength range of 3900–6900 Å. The total integration time for cluster galaxies was typically 10–20 minutes. The redshifts listed in Table 3 were obtained using the cross-correlation technique of Tonry and Davis (1979).

These measurements, even coupled with the published measurements of Faber and Dressler (1977); Melnick and Quin-

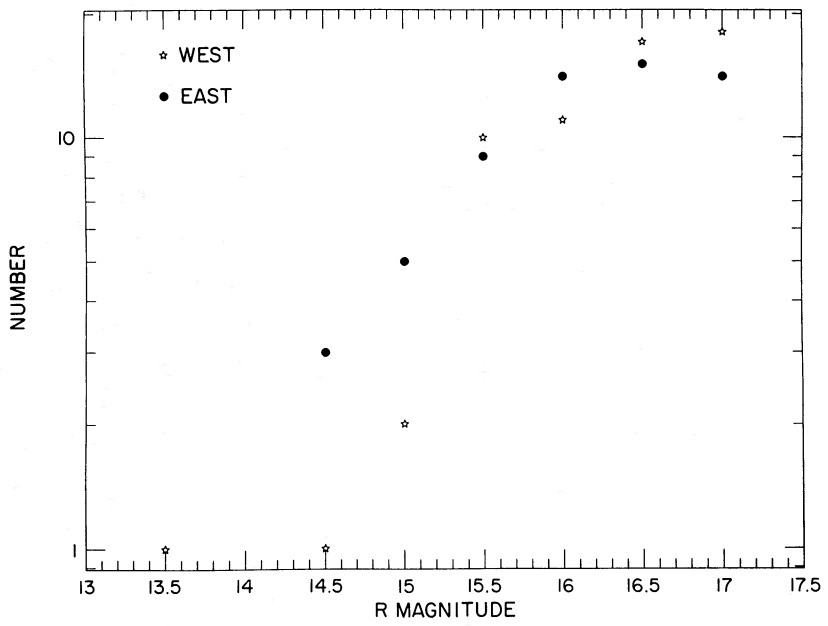

FIG. 3.—The galaxy luminosity functions for the east and west condensations. Note that the western clump which contains the cD has a deficit of other bright galaxies.

© American Astronomical Society • Provided by the NASA Astrophysics Data System

1986ApJ...308..530F

PLATE 11

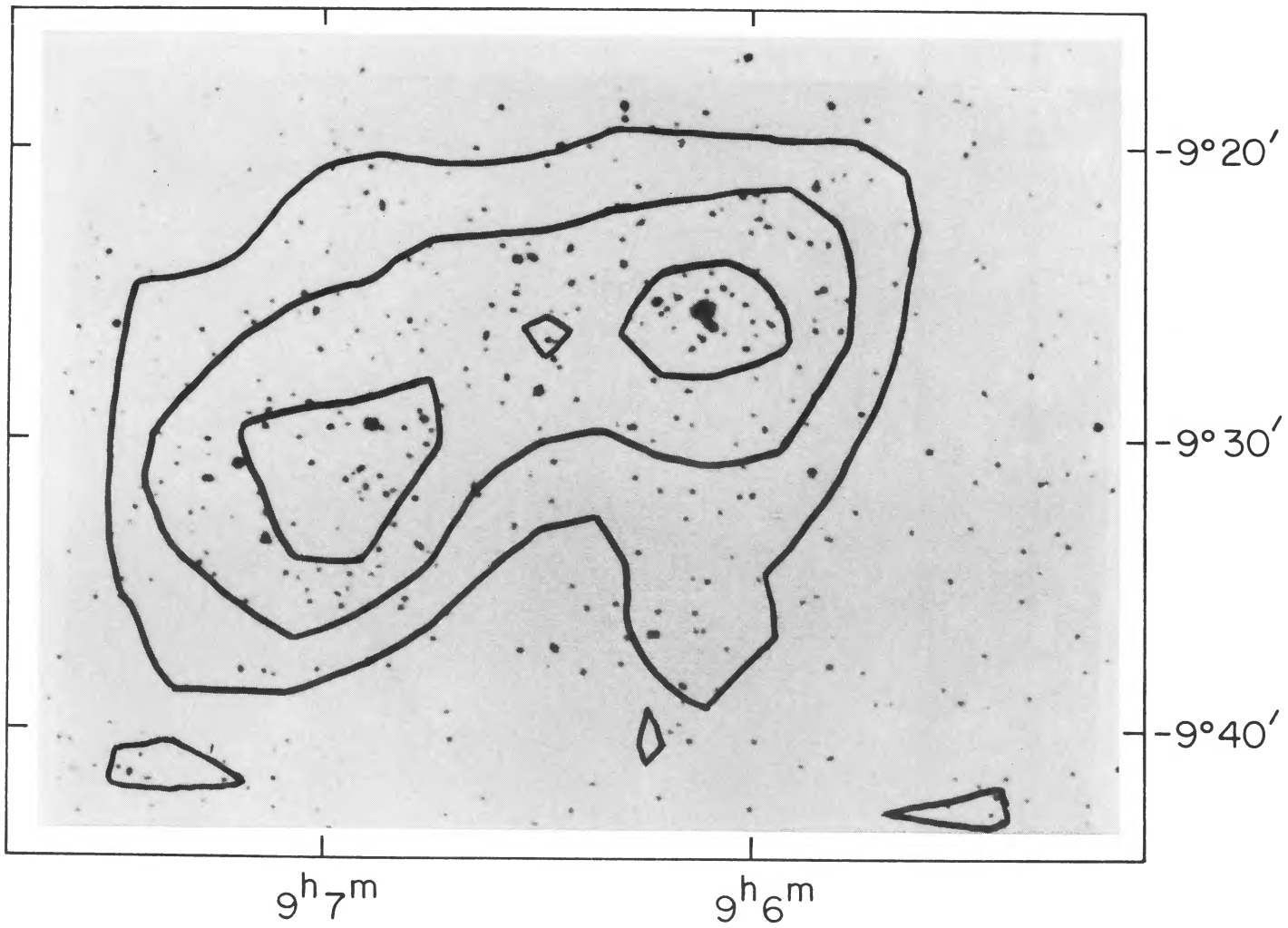

FIG. 2.—A contour plot of galaxy surface density in A754 superposed on an image processed from a POSS E plate. The stars have been removed from this image as described in the text; the faintest galaxies shown have $M_R = 18.8$. The contours for the galaxy counts are smoothed by a 4′ Gaussian. The levels plotted are 1440, 2160 and 2880 galaxies deg^{-2}.

FABRICANT *et al.* (*see* page 533)

© American Astronomical Society • Provided by the NASA Astrophysics Data System

1986ApJ...308..530F

TABLE 3

HELIOCENTRIC VELOCITIES FOR GALAXIES IN ABELL 754

Number	R.A. (1950)	Decl.	Velocity	Source[a]
25.....	09^{h}05^{m}36^s.4	−09°47′25″	16035 ± 38	T
43.....	09 06 27.3	−09 37 32	15091 ± 49	T
52.....	09 07 17.9	−09 31 43	15123 ± 44	MMT
54.....	09 07 09.7	−09 32 12	15731 ± 50	MMT
55.....	09 07 08.7	−09 32 54	16234 ± 35	MMT
56.....	09 07 09.0	−09 33 21	15998 ± 31	MMT
58.....	09 06 46.2	−09 34 03	15792 ± 88	MMT
63.....	09 07 17.9	−09 30 18	16625 ± 43	MMT
66.....	09 06 59.0	−09 29 53	15741 ± 39	MMT
67.....	09 06 53.1	−09 29 47	16255 ± 38	MMT
85.....	09 06 36.6	−09 26 34	17181 ± 66	MMT
86.....	09 06 32.5	−09 25 02	17336 ± 48	MMT
88.....	09 06 30.1	−09 23 42	14455 ± 36	MMT
91.....	09 06 06.2	−09 25 37	16347 ± 37	MMT
92.....	09 09 05.3	−09 26 14	15813 ± 33	MMT
105.....	09 06 24.9	−09 23 24	15792 ± 50	MMT
...	09 06 27.9	−09 26 44	15809 ± 47	MMT

[a] T, Tillinghast 1.5 m reflector; MMT, Multiple Mirror Telescope.

tana (1981); and Harris, Costain, and Dewdney (1984), do not provide a reliable estimate of the mean velocities and dispersions of the two subcondensations in the cluster center. We have, however, made estimates based on a sample of 88 velocities measured by S. Shectman and A. Dressler. These velocities were kindly provided to us in advance of publication (Dressler 1985).

Within our ability to eliminate foreground/background contamination, the mean velocities and velocity dispersions of the clumps are identical to each other and to the results from the whole Shectman and Dressler sample. Eliminating a single foreground galaxy from the samples, we obtain (all in km s^{-1}) for the whole region $\langle v \rangle = 16{,}276 \pm 80$, $\sigma = 750^{+68}_{-55}$ (87 galaxies); for the eastern clump $\langle v \rangle = 16{,}145 \pm 160$, $\sigma = 733^{+156}_{-102}$ (21 galaxies); and for the western clump $\langle v \rangle = 16{,}165 \pm 217$, $\sigma = 839^{+223}_{-132}$ (15 galaxies). These estimates may be affected by background contamination. Shectman and Dressler (1986) will contain a more detailed analysis of the velocity data.

IV. X-RAY ESTIMATION OF THE MASS DISTRIBUTION

The flattened, apparently bimodal galaxy distribution in A754 (Fig. 2; see also Baier 1979; Melnick and Quintana 1981; Beers 1983) suggests a simple model for the mass distribution which consists of two self-gravitating isothermal spheres separated by ~12′ on the sky. The corresponding projected separation is $R_p = 0.56$ Mpc. The asymmetric, flattened X-ray surface brightness distribution (Fig. 1) is inconsistent with an underlying smooth ellipsoidal mass distribution. In this section we examine fits to the X-ray data of the model suggested by the galaxy distribution. We refine the model parameters by calculating an extensive grid of model mass distributions for comparison with the X-ray data. In the next section we make a detailed comparison between these models and the galaxy position data.

We consider two extreme geometries. If the spatial separation of the centers of the two clumps is R, these two geometries have $R \approx R_p$ (clumps separated mainly in the plane of the sky) and $R \gtrsim 5R_p$ (clumps separated mainly along the line of sight). The factor of 5 is a convenient fiducial factor for which the clumps are spatially well separated in all fits to the X-ray data. We now model these two cases and show that the X-ray data are inadequate to distinguish between them (or, obviously, among intermediate models). In the next two sections we show that the optical position and velocity data are also consistent with either geometry.

We first consider the case $R \approx R_p$. In this case, the sound crossing time for the X-ray emitting gas is comparable to the free-fall time for the system of galaxies. The X-ray surface brightness distribution could thus be somewhat affected by departures from hydrostatic equilibrium, but we expect these departures to be small.

We calculate the X-ray surface brightness for an isothermal X-ray emitting gas in hydrostatic equilibrium in the gravitational potential of the mass distribution of two overlapping isothermal spheres. We implicitly assume that the gas contributes a negligible fraction of the cluster mass. At each point along a particular line of sight through the cluster, we calculate the summed potential from the two isothermal sphere mass distributions (Chandrasekhar and Wares 1949 contains a useful tabulation of the gravitational potential for a self-gravitating isothermal sphere). The equation of hydrostatic equilibrium

$$\nabla p_{\rm gas} = -\rho_{\rm gas} \nabla \phi$$

and the ideal gas law

$$p_{\rm gas} = \rho_{\rm gas} kT/\mu m_{\rm H}$$

yield a relation between the gas density and the gravitational potential

$$\rho_{\rm gas} = \rho_{\rm gas}(0) \exp \{-\mu m_{\rm H}[\phi(r) - \phi(0)]/kT\} .$$

In these equations ϕ is the gravitational potential, $p_{\rm gas}$ is the gas pressure, $\rho_{\rm gas}$ is the gas density, T is the gas temperature, $m_{\rm H}$ is the proton mass, and μ is the mean molecular weight. The X-ray surface brightness is then proportional to the integral of $\rho^2_{\rm gas}$ along the line of sight.

In the grid of models for comparison with the X-ray data, we vary the core radii of the two isothermal spheres, the spacing between their centers, and the parameter β ($\equiv \langle v^2 \rangle \mu m_{\rm H}/3kT$), which is the ratio of the square of the galaxy velocity dispersion to the X-ray emitting gas temperature. We assume the same β for both clumps.

We use the moments of the plane figures bounded by the model isophotes (spaced by a factor of 1.5 in surface brightness as for the data) to assess the agreement between the model and the data. We compare the modeled and observed surface brightness profile, the movement of the isophote center as a function of surface brightness, and the axial ratio as a function of surface brightness. Although the model parameters are not completely independent, the axial ratio of the modeled isophotes and the movement of the isophote centers are most sensitive to the separation of the two clumps, and the surface brightness profile is most sensitive to the core radii and the value of β. Figures 4 and 5 show the corresponding surface brightness distributions and projected mass distributions respectively. Figure 6 shows comparisons between two models and the data. The two models we display span a conservative range of the model parameters which are allowed by our necessarily qualitative assessment of the errors in the fitting procedure.

For these models, the core radius of the eastern clump is between 2.′5 and 3.′0, that of the western between 5.′0 and 7.′0. The separation of the clumps is in the range 10′–12′, and the parameter β is in the range 0.41–0.45. The value of $\beta \equiv \beta_i$, independently determined from the observed velocity disper-

© American Astronomical Society • Provided by the NASA Astrophysics Data System

1986ApJ...308..530F

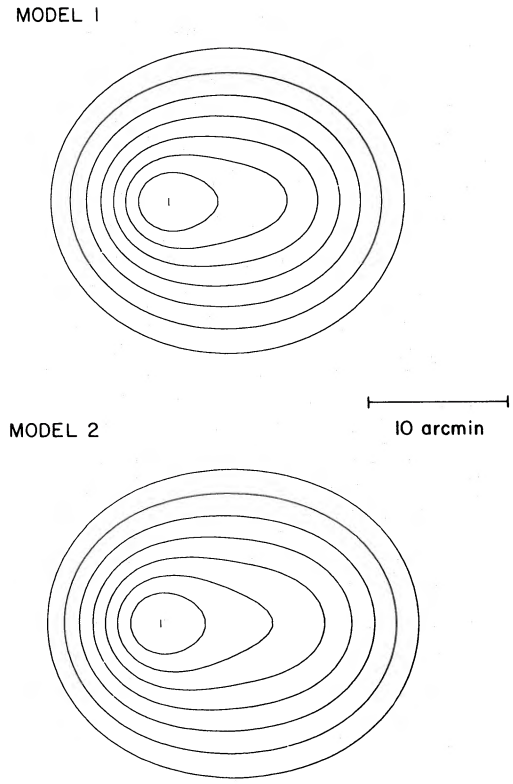

FIG. 4.—Modeled surface brightness profiles for comparison with Fig. 1. The contour levels are separated by a factor of 1.5. Model 1 is the surface brightness calculated from the equilibrium distribution of gas in the potential of two isothermal spheres with core radii of 2.5 and 5.0, separated by 10′. The parameter β is 0.41. Model 2 has two clumps with core radii of 2.8 and 6.0 separated by 12′; β is 0.45. Both model 1 and model 2 pertain to the situation where $R \approx R_p$ (clumps separated mainly in the plane of the sky).

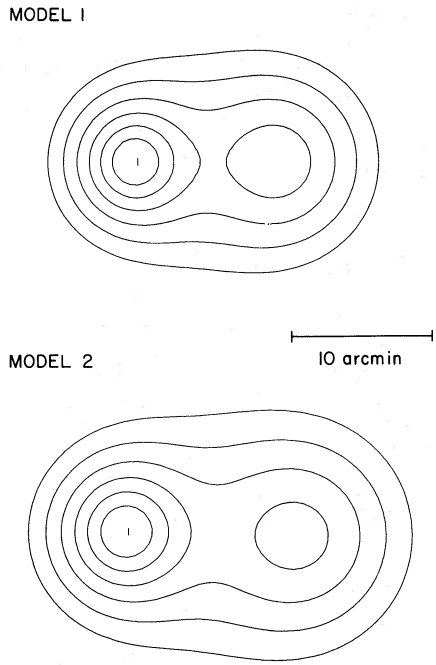

FIG. 5.—The projected mass distributions of the two models described in Fig. 3. The contour levels are separated by a factor of 1.33, the spacing between the two higher contour levels in Fig. 2. Model 1 and model 2 are the same as in Fig. 4.

sion and X-ray emitting gas temperature (5.5–9 keV), falls in the range 0.32–0.83. The quoted error arises from the 1 σ variations in the velocity dispersion for the entire sample of 87 galaxies and from the uncertainty in the gas temperature.

In the second case, where $R \gtrsim 5R_p$, the spatial overlap of the mass distributions is negligible and the emission arises from two spherically symmetric gas distributions. The X-ray surface brightness distribution is the superposition of two spherically symmetric surface brightness distributions with $I \propto (1 + r^2/a^2)^{-3\beta+1/2}$, where a is the core radius and β is defined above. For simplicity, we take the same β for both clumps.

In this case, the core radius of the eastern clump is between 3.5 and 4.5, that of the western clump is between 6′ and 8′, and the separation between the two clumps is between 7′ and 9′. The ranges for the core radii overlap with the results for the case $R \approx R_p$, and the separation is somewhat smaller. The ratio of the central surface brightnesses of the two clumps is $\sim$2.5. The parameter β is in the range 0.7–0.85. The best-fitting models fit the data less well than those for the case $R \approx R_p$ (Figures 4–6), but the fits could be improved by taking different β in the two clumps.

So far we have assumed isothermality. This assumption is reasonable for a study limited to the cluster core. Even for the extreme assumption of an adiabatic polytrope, the temperature variation over a core radius is only a factor of 2. This variation changes the interpretation of the parameter β. For an adiabatic polytrope, the effective temperature would be higher than the 8 keV derived from the integrated spectrum for the cluster. However, we find good agreement between β_i and the β fitted in the $R \approx R_p$ models. For $R \gtrsim 5R_p$, the β we obtain is larger than β_i; a polytropic model cannot improve the agreement.

From the models for the gas and mass density distributions, we can calculate the central densities and integral mass in the two components. We quote values for the case $R \approx R_p$ with a 12′ clump separation, and with core radii of 2.8 and 6.0. Note that the integral quantities are actually insensitive to the model parameters over the allowed ranges. The peak gas electron density is 1.7×10^{-3} cm^{-3}. The central mass densities in the clumps with 2.8 and 6.0 core radii are 3.8×10^{-25} and 8.2×10^{-26} g cm^{-3} respectively. The integral gas mass is $1.6 \times 10^{13}\ M_\odot$ in a volume $1.39 \times 0.65 \times 0.65$ Mpc centered between the two clumps and with the long axis parallel to the line joining their centers. (We quote masses in this unusual region for consistency with our optical coverage, which is truncated to the north by the plate boundary.) The integral mass in this volume is $2.9 \times 10^{14}\ M_\odot$; the gas mass in the cluster core is 6% of the total.

V. COMPARISON WITH OPTICAL DATA: THE V'/V'_{max} TEST

It is not yet clear whether galaxies in clusters trace the overall mass distribution. Previous comparisons of the X-ray and optically derived mass estimates indicate that the galaxies and the X-ray emitting gas trace the same matter distribution with admittedly large uncertainties (e.g., Fabricant, Rybicki, and Gorenstein 1984). We use the V'/V'_{max} test (Schmidt 1968; Avni and Bahcall 1980) to evalute the consistency of the galaxy positions in A754 with the projected mass distribution derived from the X-ray data.

In all applications of the test, we draw the galaxies from a rectangular region of 30′ × 14′ aligned with the cluster major axis. We treat the galaxies as identical test particles. This uniform weighting is equivalent to the assumptions that either

© American Astronomical Society • Provided by the NASA Astrophysics Data System

1986ApJ...308..530F

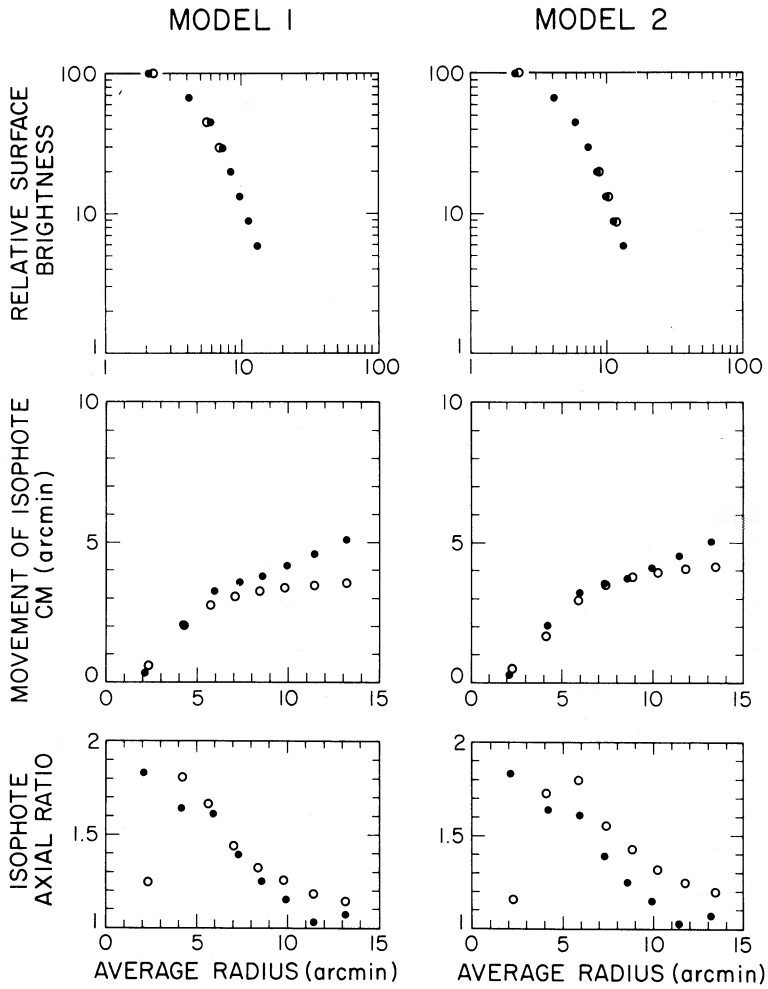

FIG. 6.—A detailed comparison between the model X-ray surface brightness distributions in Fig. 3 and the data in Fig. 1. We compare the surface brightness profiles, the movement of the isophote center of mass, and the isophote axial ratios, all as a function of average radius. Table 1 lists these quantities for the data. Filled circles refer to the data, open circles to the models. Model 1 and model 2 are the same as in Fig. 4.

the dark matter is not tied to individual galaxies, or that it is equally tied to the galaxies regardless of luminosity.

There are three parts to the test. For each of n galaxies at positions (x_n, y_n) which follow a surface density distribution $S(x, y)$, we calculate

$$\left[\frac{V'}{V'_{\max}}\right]_y = \frac{\int_{-\infty}^{y_n} dy S(x_n, y)}{\int_{-\infty}^{\infty} dy S(x_n, y)},$$

$$P(x) = \int_{-\infty}^{\infty} dy S(x, y),$$

$$\left[\frac{V'}{V'_{\max}}\right]_x = \frac{\int_{-\infty}^{x_n} dx P(x)}{\int_{-\infty}^{\infty} dx P(x)}.$$

The galaxy data need not be binned to apply this test. When applying this test to a real sample with finite spatial coverage, the limits of integration must be restricted to the available region.

The statistical basis of the $V'/V'_{\max}$ test is the general result that the cumulants of a distribution function are uniformly distributed between 0 and 1. For a consistent model, the quantities $[V'/V'_{\max}]_x$ and $[V'/V'_{\max}]_y$ are uniformly distributed between 0 and 1, and they are uncorrelated. We test the uniform distribution between 0 and 1 with the Kolmogorov-Smirnov test and the absence of correlation with the Kendall rank correlation test.

The $V'/V'_{\max}$ test yields three independent probabilities that a random sample drawn from the distribution S could produce at least as large a deviation (the two K-S tests for the x- and y-coordinates) or as large a correlation (the Kendall rank test). To reject a model with an overall confidence level of 90%, it must attain a probability for at least one of the three tests of less than $1 - (0.9)^{1/3}$, or less than 3.5%.

To compare the galaxy distribution with the mass models derived from the X-ray data, they must be registered with respect to each other. Because the peak of the X-ray surface brightness is coincident with the center of the eastern clump, we have a convenient reference point. The registration is then determined by finding the position angle of the line joining the two clumps. Table 1 shows that the position angle is $\sim 100°$. The positions derived from the IPC are accurate to 35″ at 90% confidence for point sources near the center of the IPC field. We allow a larger 1′ error for finding the peak of an extended distribution.

The background galaxy surface density is another uncertainty in comparing the models with the galaxy map. The

© American Astronomical Society • Provided by the NASA Astrophysics Data System

1986ApJ...308..530F

background estimates are ~20% to $m_R = 17.8$ and 5% to $m_R = 16.8$ (Beers, Geller, and Huchra 1982). The corners of the 45′ × 45′ field (see Kurtz 1983) give an upper limit of 34%.

Table 4 includes the results of a number of V'/V'_{max} runs comparing the red galaxy sample with the X-ray–derived models. The variables are the centering, galaxy background, and magnitude cutoff. Figure 7 shows a sample V'/V'_{max} plot.

The tests show that: (1) All the models consistent with the X-ray data are also consistent with the galaxy counts to limiting magnitudes of 16.8 and 17.8. (2) The best-fitting position angle is near 110° with an error of ~10°, in good agreement with the X-ray derived angle. (3) The fits are sensitive to changes in the registration at the 1′ level. (4) The fits are insensitive to the background level. This insensitivity would decrease if we had counts extending over a larger spatial region.

VI. DYNAMICAL CONSIDERATIONS

The X-ray brightness distribution and the galaxy surface density distribution both show that the cluster A754 contains (at least) two subcondensations. The condensations are separated by $R_p \approx 0.56$ Mpc on the sky, and the difference in the mean line-of-sight velocities of the clumps $V_r = 20 \pm 270$ km s^{-1} (Dressler 1985). For each of the clumps we take a mass of $1.8 \times 10^{14}\ M_\odot$ within a 0.56 Mpc radius, representative of the range of fits to the X-ray surface brightness.

Following the simple model proposed by Beers, Geller, and Huchra (1982) for A98 (note that there is a typographical error in eq. [13a] of that paper; the denominator should be V_∞^2), we can study A754 as a two-body system in which the clumps of galaxies are on a linear orbit and are approaching (or receding from) each other for the first time. Of course, many other more complex orbits are possible. Figure 8 shows the allowed orbital parameters as a function of V_r and α, the angle between the line connecting the clumps and the plane of the sky. Unbound solutions lie to the right of the dashed curve; there are no unbound solutions within 3 σ of the measured V_r. Changing the system mass by a factor of 2 does not affect the character of the derived solutions. Even if we more substantially underestimate the mass, the small observed velocity difference limits the system to states very near maximum expansion or coalescence.

For $V_r = 20$ km s^{-1}, there are three bound solutions. For two of these solutions (both with $\alpha \approx 84°$), the system is near maximum expansion. The spatial separation of the clumps is ~5 Mpc (i.e., $R \gtrsim 5R_p$). The steep projection angle may not be surprising, because the identification of double clusters from the X-ray data is strongly biased toward systems which have a small separation projected on the sky. In the third solution ($\alpha = 0.°5$) the clumps are separated by 0.56 Mpc ($R \approx R_p$), and the time to coalescence is comparable to the crossing time for an individual clump ($t_c \approx 4 \times 10^8$ yr). For massive clumps, the time of coalescence is shorter. In this case our simple model breaks down in detail, because we treat the clumps as point masses.

The N-body simulations of Cavaliere *et al.* (1985) indicate that the two-body model is a good approximation for systems which are dominated by two concentrations. Their models also predict that a significant fraction of clusters as massive as A754 should be near maximum expansion now; the dynamical evolution of these systems is slowed by the formation and persist-

TABLE 4

V'/V'_{max} RESULTS

Center	Background	Magnitude Limit m_R	$P(x)$	$P(y)$	P_{cor}	Remarks
		$R \approx R_p$ Model				
Varying the center (~135 galaxies):						
$9^h6^m27^s.3$, −9°26′33″.....	20%	17.8	0.22	0.06	0.06	Nominal
9 6 30.2, −9 25 50	20	17.8	0.46	0.0005	0.07	
9 6 24.4, −9 25 50	20	17.8	0.04	0.01	0.06	
9 6 26.2, −9 27 15	20	17.8	0.09	0.36	0.12	
9 6 30.2, −9 27 15	20	17.8	0.72	0.32	0.10	
Varying the background (~135 galaxies):						
$9^h6^m30^s.2$, −9°27′15″.....	10%	17.8	0.63	0.33	0.10	
9 6 30.2, −9 27 15	20	17.8	0.72	0.32	0.10	Nominal
9 6 30.2, −9 27 15	40	17.8	0.74	0.30	0.10	
9 6 30.2, −9 27 15	100	17.8	0.20	0.04	0.11	Uniform distribution
Varying the magnitude limit (~74 galaxies):						
$9^h6^m30^s.2$, −9°27′15″.....	5%	16.8	0.54	0.39	0.22	
		$R \gtrsim 5R_p$ Model				
Varying the center (~135 galaxies):						
$9^h6^m34^s.9$, −9°27′14″.....	20%	17.8	0.02	0.06	0.10	Nominal
9 6 37.8, −9 26 31	20	17.8	0.01	0.0003	0.09	
9 6 32.0, −9 26 31	20	17.8	0.15	0.01	0.09	
9 6 32.0, −9 27 56	20	17.8	0.02	0.18	0.17	
9 6 37.8, −9 27 56	20	17.8	0.006	0.22	0.12	
9 6 30.9, −9 27 14	20	17.8	0.17	0.22	0.11	
Varying the magnitude limit (~74 galaxies):						
$9^h6^m30^s.9$, −9°27′14″.....	5%	16.8	0.12	0.18	0.22	

NOTE.—P.A. = 110°. For $R \approx R_p$, the model tested is two projected isothermal spheres with core radii of 2.′8 and 6.′0, separated by 12′. For $R \gtrsim 5R_p$, we take core radii of 4.′0 and 7.′0 separated by 8′. The central densities of the projected distributions are related by the inverse ratio of their core radii, as their velocity dispersions are assumed to be identical. Note that the movements for the cases where the center is varied are along a circle of radius 1′ surrounding the nominal center.

© American Astronomical Society • Provided by the NASA Astrophysics Data System

1986ApJ...308..530F

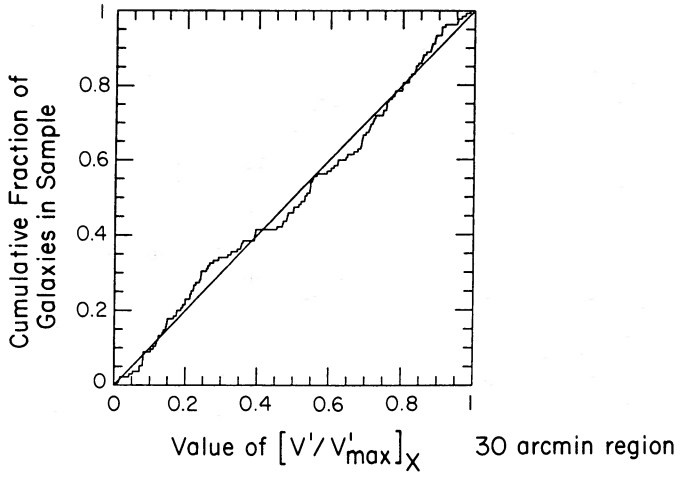

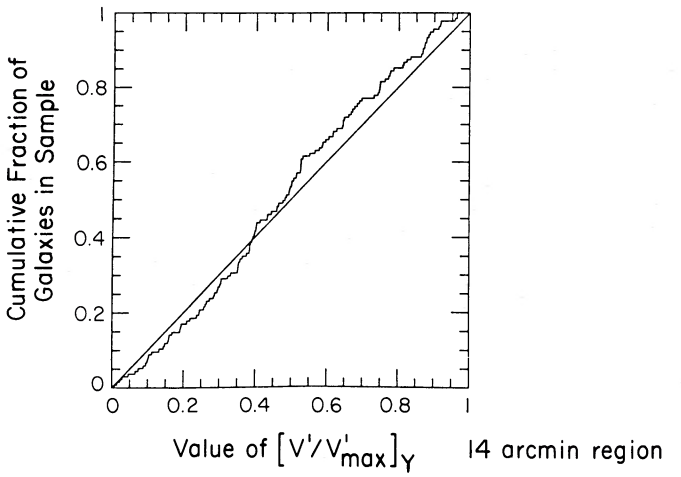

FIG. 7.—Plots of the cumulative V'/V'_{max} distributions for the $R \approx R_p$ model with two clumps of core radius 2.'8 and 6.'0, separated by 12'. The fraction of background galaxies is 20%. The midpoint of the line joining the two clumps is centered at R.A. $9^h6^m20^s.2$, Decl. $-9°27'15''$, with a position angle of 110°.

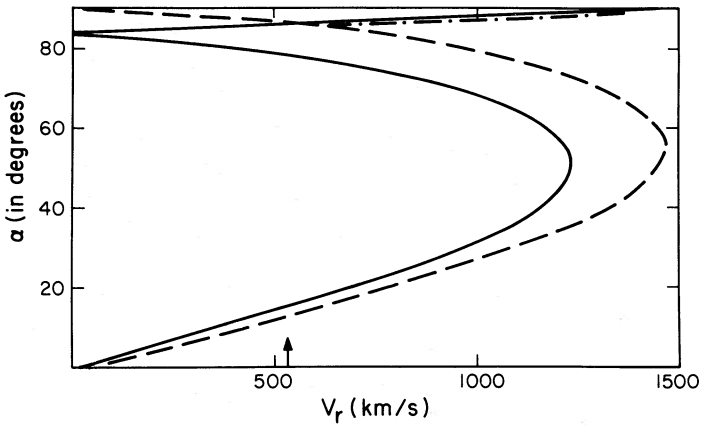

FIG. 8.—Projection angle as a function of radial velocity V_r for two clumps on a linear orbit. *Solid curve*, solutions for linear orbits; *dashed curve* separates regions of bound and unbound solutions; *dot-dash curve*, Hubble flow.

ence of large substructures. With the available data we cannot determine whether a cluster like A754 is really near maximum expansion or whether we have caught it shortly before coalescence. However, detailed data on large, well-understood cluster samples could provide statistical constraints on the dynamical state of rich clusters.

VII. SUMMARY AND CONCLUSIONS

Both X-ray and optical data show that A754, a system comparable to the Coma Cluster, is (at least) bimodal. The X-ray surface brightness profile can be produced by an isothermal ($T \approx 8$ keV) gas in hydrostatic equilibrium in the gravitational potential of two self-gravitating isothermal spheres. Application of the V'/V'_{max} test shows that the galaxies trace this mass distribution. In other words, on a scale of 0.5–1 Mpc, the galaxies trace the smoothed distribution of dark matter in the system. The X-ray and optical estimates of the mass in the central region of the cluster are $\sim 2.9 \times 10^{14}$ and $3.6 \pm 0.5 \times 10^{14}$ $M_\odot$ respectively. The mass-to-light ratio (using the X-ray mass and the corrected blue light) is 445 in solar units. The X-ray emitting gas contributes $\sim 6\%$ of the mass, and the luminous material in galaxies contributes another 5%.

The N-body simulations by Cavaliere *et al.* (1985) produce systems which bear a remarkable resemblance to A754. The dissipationless hierarchical gravitational instability picture thus appears to offer an explanation of the structure we observe on these scales. In this picture, clusters in a particular mass range (e.g., A754 and Coma) exhibit a wide range of morphologies which correspond to a range of "dynamical ages." The clumpiness of a system we observe *now* is a result of the discreteness of the galaxies in the system during the *early* stages of cluster evolution. Measurement of the fraction of clusters (as a function of mass or density) which retain substructure would provide a detailed test of the validity of these models.

The difficulty of uncovering and understanding substructure in clusters increases as the spacing of the subclumps decreases. In the absence of systematic redshift differences across the cluster, the only optical clue is the clumpiness of the galaxy distribution. With the relatively small numbers of cluster members and the problems of background contamination, the X-ray data is particularly important. A754 is a case in point.

Our fits to the X-ray surface brightness map are based on a number of simplifying assumptions. We assume that the X-ray emitting gas is isothermal and in hydrostatic equilibrium. Future X-ray missions like LAMAR and AXAF will provide the spatially resolved spectra needed to provide further constraints on the physics of these systems.

This research was supported in part by NASA contract NAS8-30751. NASA grant NAGW-201, and a grant from the Smithsonian Institution Scholarly Studies Program. We thank Y. Avni for suggesting the use of the V'/V'_{max} test and for assistance in its application.

REFERENCES

Abell, G. 1958, *Ap. J. Suppl.*, **3**, 211.
Abramopoulos, F., and Ku, W. 1983, *Ap. J.*, **271**, 446.
Avni, Y., and Bahcall, J. 1980, *Ap. J.*, **235**, 694.
Baier, F. W. 1976, *Astr. Nach.*, **297**, 295.
———. 1979, *Astr. Nach.*, **300**, 133.
Beers, T. C. 1983, Ph.D. thesis, Harvard University.

© American Astronomical Society • Provided by the NASA Astrophysics Data System

1986ApJ...308..530F

Beers, T. C., and Geller, M. J. 1983, *Ap. J.*, **274**, 491.
Beers, T. C., Geller, M. J., and Huchra, J. P. 1982, *Ap. J.*, **257**, 23.
Bothun, G. D., Geller, M. J., Beers, T. C., and Huchra, J. P. 1983, *Ap. J.*, **268**, 47.
Burstein, D., and Heiles, C. 1982, *A.J.*, **87**, 1165.
Cavaliere, A., Santangelo, P., Tarquini, G., and Vittorio, N. 1985, preprint.
Chandrasekhar, S., and Wares, G. 1949, *Ap. J.*, **109**, 551.
Davis, M., and Huchra, J. P. 1982, *Ap. J.*, **245**, 437.
Dressler, A. 1980, *Ap. J. Suppl.*, **42**, 565.
Dressler, A. 1985, private communication.
Faber, S. M., and Dressler, A. 1977, *A.J.*, **82**, 187.
Fabricant, D., Rybicki, G., and Gorenstein, P. 1984, *Ap. J.*, **286**, 186.
Forman, W., Bechtold, J., Blair, W., Giacconi, R., Van Speybroeck, L., and Jones, C. 1981, *Ap. J. (Letters)*, **243**, L133.
Forman, W., and Jones, C. 1982, *Ann. Rev Astr. Ap.*, **20**, 547.
Geller, M. J. 1984, *Comments Ap.*, **10**, 47.
Geller, M. J., and Beers, T. C. 1982, *Pub. A.S.P.*, **94**, 421.
Harnden, F., Jr., Fabricant, D., Harris, D., and Schwartz, J. 1984, *SAO Spec. Rep.*, No. 393.
Harris, D., ed. 1984, *Einstein Observatory Revised Users Manual.*
Harris, D. E., Costain, C. H., and Dewdney, P. E. 1984, *Ap. J.*, **280**, 532.
Heiles, C. 1975, *Astr. Ap. Suppl.*, **20**, 37.
Kurtz, M. J. 1983, in *Statistical Methods in Astronomy*, ed. E. Rolfe (ESA Spec. Pub. SP201), p. 47.
Kurtz, M. J., Huchra, J. P., Beers, T. C., Geller, M. J., Gioia, I. M., Maccacaro, T., Schild, R. E., and Stauffer, J. R. 1985, *A.J.*, **90**, 1665.
Latham, D. W. 1979, in *The MMT and the Future of Ground Based Astronomy*, ed. T. C. Weekes (Cambridge: Smithsonian Astrophysical Observatory, *Spec. Rept.*, No. 385), p. 119.
Melnick, J., and Quintana, H. 1981, *Astr. Ap. Suppl.*, **44**, 87.
Mushotzky, R. 1982, paper presented at Nice Workshop on Hot Astrophysical Plasmas.
Oemler, A. J. 1974, *Ap. J.*, **194**, 1.
Schecter, P. 1976, *Ap. J.*, **203**, 297.
Schild, R., and Oke, J. B. 1971, *Ap. J.*, **169**, 209.
Schmidt, M. 1968, *Ap. J.*, **151**, 393.
Shectman, S., and Dressler, A. 1986, in preparation.
Tonry, J., and Davis, M. 1979, *A.J.*, **84**, 1511.

TIMOTHY BEERS: Astronomy Department, California Institute of Technology, Pasadena, CA 91125

DANIEL FABRICANT, MARGARET GELLER, PAUL GORENSTEIN, JOHN HUCHRA, and MICHAEL KURTZ: Harvard-Smithsonian Center for Astrophysics, 60 Garden Street, Cambridge, MA 02138

© American Astronomical Society • Provided by the NASA Astrophysics Data System